Geophys. J. Int. (2002) **149,** 364–373

Non-double-couple earthquakes of 1997 January in West Bohemia, Czech Republic: evidence of tensile faulting

Václav Vavryčuk

Geophysical Institute, Academy of Sciences of the Czech Republic, Boční II/1401, 141 31 *Praha* 4, *Czech Republic. E-mail: vv@ig.cas.cz*

Accepted 2001 November 11. Received 2001 October 26; in original form 2001 February 6

SUMMARY

A mixed family of double-couple (DC) and non-double-couple (non-DC) earthquakes was observed during the 1997 January earthquake swarm in West Bohemia, which is a geothermal region typical for the occurrence of earthquakes swarms. The DC and non-DC earthquakes occurred within a small area of less than 1 km^3 on faults of different orientations. The stress in the area is determined from focal mechanisms and attains values (plunge/azimuth): $\sigma_1 = 33^\circ/156^\circ$, $\sigma_2 = 48^\circ/20^\circ$, $\sigma_3 = 23^\circ/262^\circ$, with a shape ratio of $R = 0.69 \pm 0.15$. The error in the stress directions (plunge/azimuth) is up to $\sim 5^\circ/10^\circ$. The absolute stress values were estimated to be $\sigma_1 = 350$ MPa, $\sigma_2 = 220$ MPa and $\sigma_3 = 162$ MPa. The lithostatic stress is 250 MPa. The stress analysis shows that the DC earthquakes occurred on optimally oriented faults (with high shear traction) but the non-DC earthquakes occurred on misoriented faults (with low shear traction). The percentage of the DC in earthquakes clearly correlates with the magnitude of shear traction: high/low DC is associated with high/low shear traction. This indicates that the type of faulting is probably controlled by tectonic stress and that the non-DC earthquakes are not related to pure shear faulting but may combine shear and tensile faulting. The tensile faulting is manifested by positive isotropic and compensated linear vector dipole components. The tensile faulting is conditioned by high pore fluid pressure, which was estimated to be approximately 244 MPa. The fluid pressure is less than the lithostatic stress by $\sim$5 MPa. The ratio of the fluid pressure to the maximum compressive stress is 0.7.

Key words: fluid pressure, moment tensors, non-double-couple mechanisms, shear faulting, tectonic stress, tensile faulting.

1 INTRODUCTION

The origin of non-double-couple (non-DC) components in earthquakes can be various (see Frohlich 1994; Julian *et al.* 1998; Miller *et al.* 1998). The non-DC components are frequently spurious, being a product of imperfect earthquake source modelling. This occurs when the amount of data is limited, when the Green functions are inaccurate (Kuge & Lay 1994), or when the source process is inadequately simplified. For example, assuming a point-source approximation for complex faulting of finite extent or for multiple faulting on faults with different orientations can produce non-DC mechanisms (Sipkin 1986). Spurious non-DC components can also be an artefact of neglecting the inhomogeneity or anisotropy of the medium (Šílený & Vavryčuk 2000). However, the non-DC mechanisms can also be real and reflect specific earthquake processes. The non-DC components in earthquakes can be caused by landslides (Hasegawa & Kanamori 1987), inflation or deflation of magma chambers in volcanic areas (Mori & McKee 1987), by tensile faulting caused by high fluid pressure in geothermal and volcanic areas (Ross *et al.* 1996; Julian *et al.* 1997), or by shear faulting in an anisotropic medium (Kawasaki & Tanimoto 1981). The non-DC components are also reported for deep earthquakes in slabs or for rock bursts in mines (Rudajev & Šílený 1985; Feigneir & Young 1992).

Since causes of non-DC components in earthquakes can be various, it is crucial to resolve in any study of non-DC components: (1) whether they are really physical or just errors of an inversion and (2) provided they are physical, which processes generated them. The aim of this paper is to answer these fundamental questions for microearthquakes, which occurred during the 1997 January West-Bohemian earthquake swarm and that often displayed high non-DC components (Dahm *et al.* 2000; Horálek *et al.* 2000b). It will be shown that the observed non-DC components are real phenomena, which can be explained consistently by tensile faulting owing to high pore fluid pressure. Evaluation of the parameters of tensile faulting is presented in a separate paper (Vavryčuk 2001).

2 THE 1997 JANUARY WEST-BOHEMIAN EARTHQUAKE SWARM

West Bohemia is a seismically active geothermal area typical for the occurrence of earthquake swarms. The seismic activity in the

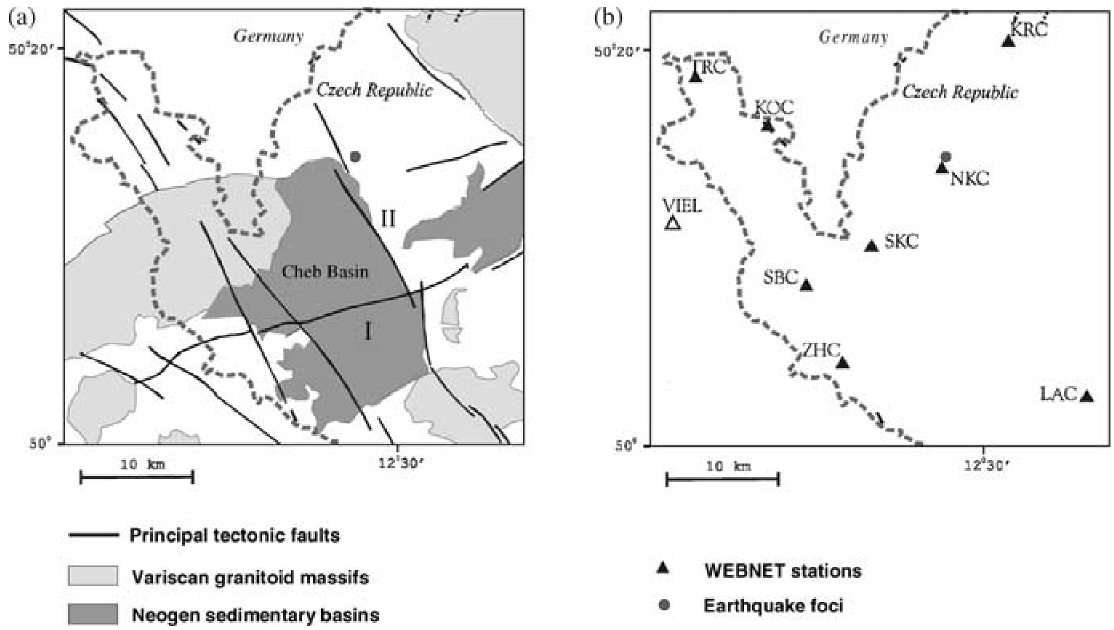

Figure 1. Tectonic sketch of the West Bohemia region (a) and positions of the seismic stations (b). (I) Ore-Mountain fault system, (II) Eastern boundary fault of the Cheb Basin. Solid triangles show the West Bohemia Network (WEBNET) seismic stations, open triangle shows the VIEL station operated in NE Bavaria by the Munich University.

area is probably connected with young Quaternary volcanism manifested by intrusions of mantle fluids and gases (Weinlich *et al.* 1998). The 1997 January earthquake swarm lasted for two weeks and involved about 1800 microearthquakes. The strongest event was of magnitude 3.0. The hypocentres clustered within a very small volume of probably less than 1 km^3 at a depth of about 9 km (Fischer & Horálek 2000). The hypocentres occurred beneath the northeastern edge of the Cheb Basin, which is situated in the northwestern part of the Bohemian Massif (Fig. 1). The crystalline basement of the Cheb Basin is covered by Tertiary sediments with a maximum thickness of 400 m. The tectonic structure of the Cheb Basin is characterized by two principal fault systems (Dudek 1987): the Sudeten NW–SE fault system and the Ore-Mountain WSW–ENE fault system. The NW–SE fault system is manifested by the Eastern boundary fault of the Cheb Basin, considered to be a continuation of the Mariánské Lázně fault (Špičák *et al.* 1999).

The microearthquakes were recorded by nine local three-component digital broad-band (0.5–60 Hz) seismic stations (see Fig. 1) with a sampling rate of 125 or 250 Hz and with a dynamic range of 96 dB or more (Horálek *et al.* 2000a). Horálek *et al.* (2000b) inspected the seismograms of the majority of the recorded events visually and classified them into eight types according to their *P* and *S* waveforms at the individual stations. The earthquakes of the two most frequent types were denoted as A and B events. The A events occurred predominantly in the beginning of the swarm, while the B events predominated at the end of the swarm. The other types of events were much rarer and represented events with rather exceptional waveforms. Fischer & Horálek (2000) located the A and B events using the master-event procedure and calculated the orientation of possible fault planes from the clustering of the foci. They suggested that the A and B events were possibly associated with two crossing faults (see Fig. 2) or fault systems, which were approximately perpendicular to each other.

3 DC AND NON-DC COMPONENTS IN EARTHQUAKES

3.1 Earthquake mechanisms

Horálek *et al.* (2000b) selected 70 earthquakes (20 type A events, 29 type B events and 21 other type events) recorded with a high signal-to-noise ratio at six to nine seismic stations. They measured the *P*- and *S*-wave amplitudes in the three-component ground displacement seismograms and calculated the full moment tensors by applying the inversion method of Šílený (1997, 1998). They determined the orientations of the double couple (DC) from the moment tensors. They found that type A events were oblique normal, and type B events oblique reverse (see Fig. 2). The A events are defined by strikes (290°, 320°), dips (40°, 60°) and rakes (−155°, −175°), and the B events by strikes (20°, 60°), dips (55°, 90°) and rakes (35°, 50°). The mechanisms in both families of earthquakes are consistent and the focal parameters vary only slightly within the family (see Fig. 2).

3.2 Definition of non-DC components

Since full moment tensors are available for selected earthquakes (Dahm *et al.* 2000; Horálek *et al.* 2000b), we can decompose them into the double-couple and non-double-couple components. The non-DC component is defined as the sum of the compensated linear vector dipole (CLVD) and isotropic (ISO) components (see Knopoff & Randall 1970; Jost & Hermann 1989). The size of the ISO, CLVD and DC can be evaluated in per cent as follows:

$$\mathrm{ISO} = \frac{1}{3}\frac{\mathrm{Tr}(\mathbf{M})}{\left|M_{|\max|}\right|} \times 100\,\text{per cent}, \tag{1}$$

$$\mathrm{CLVD} = -2\frac{M^*_{|\min|}}{\left|M^*_{|\max|}\right|}(100\,\text{per cent} - |\mathrm{ISO}|), \tag{2}$$

$$\mathrm{DC} = 100\,\text{per cent} - |\mathrm{ISO}| - |\mathrm{CLVD}|, \tag{3}$$

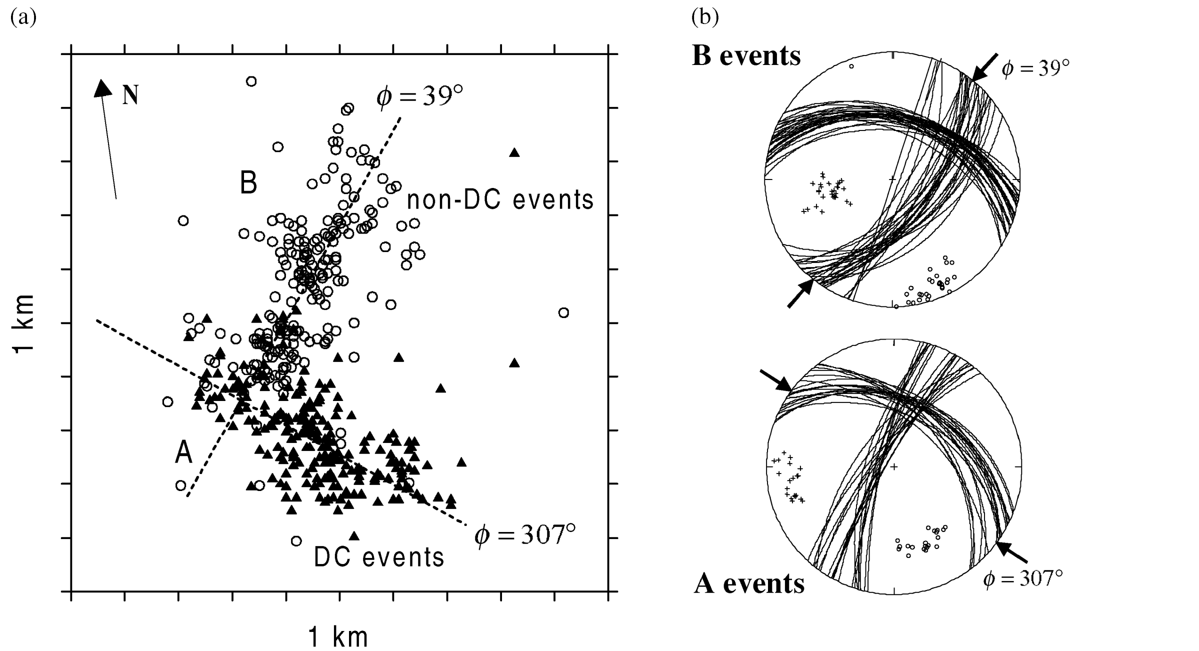

Figure 2. Epicentres of the type A (triangles) and B (circles) events of the 1997 January earthquake swarm (a) and the mechanisms for the selected events (b). The dashed lines and arrows show the fault plane orientations estimated by visual interpolation of foci clusters, ϕ denotes the strike of the fault planes. The circles and crosses in the right-hand plot show the *P*- and *T*-axes, respectively. The lower hemisphere equal-area projection is used.

where Tr(**M**) denotes the trace of the seismic moment tensor **M**, $M_{|\max|}$ denotes the eigenvalue of **M** that has the maximum absolute value, and $M^*_{|\max|}$ and $M^*_{|\min|}$ are the eigenvalues of the deviatoric moment tensor with the maximum and minimum absolute values, respectively.

Eqs (1)–(3) imply that the ISO and CLVD components can be either positive or negative, but the DC component is always positive. The plus/minus signs of the ISO and CLVD components express the explosive/implosive or tensile/compressive character of the source. The sum of absolute values of DC, ISO and CLVD is 100 per cent. A detailed discussion of advantages of the decomposition (1)–(3) compared with other decompositions is given in Vavryčuk (2001).

3.3 Values of non-DC components and their reliability

The decomposition of the full moment tensors into ISO, CLVD and DC for selected earthquakes (see Tables 1 and 2) shows that the A and B events differ not only in the orientation of the double couple, but they also exhibit a different percentage of the DC and non-DC components (see Fig. 3). The A events contain predominantly a high DC (with typical values from 80 to 90 per cent), while the B events contain predominantly a low DC (with typical values from 40 to 60 per cent). The non-DC components consist of both isotropic and compensated linear vector dipole parts. The CLVD is tensile/compressive for 28/1 type B events and for 10/10 type A events. The ISO is explosive for all B events and explosive/implosive for 12/8 type A events. Hence the A events are predominantly DC events with low positive or negative values of ISO and CLVD, while the B events are highly non-DC with only positive values of ISO and CLVD. The only exception is B event no 27, which has a small negative value of CLVD.

Obviously, we are faced with the question of whether the non-DC components detected are reliable or just errors of the inversion owing to the data limitation. Dahm *et al.* (2000) explored the accuracy of the mechanisms of the events by comparing absolute and relative moment tensor solutions. They estimated errors caused by inaccurate amplitudes and mismodelling of the medium. Their analysis indicates that the non-DC components in the B events are significant at a high confidence level and cannot be produced by inaccurate moment tensor inversion. Furthermore, all moment tensors were calculated using the same Green function, thus errors of the inversion owing to an oversimplified Green function should project into the moment tensors of the A events as well as of the B events but not into the moment tensors of the B events only. Hence, we conclude that: (1) the non-DC components in the majority of the A events are small and thus it is difficult to decide reliably whether they are real or spurious and (2) the non-DC components in the B events are high enough to exclude the possibility of just being errors arising from the inversion. Therefore, a significant part of these components should reflect specific properties of the source or medium.

4 POSSIBLE CAUSES OF THE NON-DC COMPONENTS

In this section we shall consider and discuss several possible causes of the non-DC components in the B type earthquakes.

4.1 Multiple shear faulting or shear faulting on a non-planar fault

If multiple shear events on different faults or shear faulting on a non-planar fault are misinterpreted as a single event, then the moment tensor of the composite event is the sum of true DC tensors, which is, in general, a non-DC tensor (Frohlich 1994). In this way, shear faulting can produce non-DC mechanisms. These mechanisms, however, never contain an ISO component. Since the trace of the composite moment tensor is the sum of traces of its components, no

Table 1. Source parameters of the A type earthquakes.

No	Date (yymmdd)	Time (hh:mm:ss)	M	δ_1 (deg)	ϕ_1 (deg)	λ_1 (deg)	δ_2 (deg)	ϕ_2 (deg)	λ_2 (deg)	α (deg)	DC (per cent)	ISO (per cent)	CLVD (per cent)
1	970115	04:57:13	1.3	46	304	−173	52	303	−175	7	94.3	5.4	0.3
2	970115	05:30:28	1.4	50	315	−167	51	315	−170	4	74.5	−6.3	−19.1
3	970115	05:30:57	1.9	43	307	−173	41	306	−176	4	86.7	−1.8	−11.5
4	970115	12:19:18	1.9	57	302	−169	47	306	−172	16	98.6	1.4	0.0
5	970115	18:10:42	1.5	49	305	−170	50	306	−173	4	96.4	0.0	3.6
6	970115	18:10:57	1.6	48	319	−166	70	310	−173	27	78.5	−2.2	−19.3
7	970115	21:03:53	0.5	45	292	−169	35	302	−172	23	92.0	0.9	7.0
8	970115	21:05:36	0.6	44	290	−168	31	302	−173	29	95.0	2.3	2.7
9	970115	21:23:03	1.3	47	297	−164	43	300	−167	9	94.8	−2.7	−2.5
10	970116	15:03:02	0.9	57	324	−152	20	144	−138	119	72.8	−3.4	−23.7
11	970116	15:11:20	2.0	61	313	−165	67	309	−153	21	71.6	−9.5	−18.9
12	970116	16:03:04	0.9	49	296	−168	52	296	−177	12	92.2	2.3	5.5
13	970116	16:12:20	1.1	56	295	−170	54	299	−174	10	81.2	6.8	12.0
14	970116	16:12:43	0.6	57	321	−159	38	133	−163	116	94.3	0.0	−5.7
15	970116	16:12:53	1.2	48	299	−160	83	83	−121	137	32.5	17.7	49.8
16	970117	05:18:35	2.0	48	304	−174	40	307	−174	11	95.0	2.2	2.8
17	970117	07:53:17	1.1	48	304	−155	45	306	−160	10	86.3	−4.8	−8.9
18	970117	21:47:36	1.4	46	297	−164	40	302	−167	15	96.5	−3.2	−0.3
19	970117	23:25:40	2.3	53	305	−170	56	304	−173	6	92.1	4.9	2.9
20	970119	02:35:42	0.6	54	323	−163	89	135	165	40	79.9	9.4	−10.7

Angles δ_1, ϕ_1 and λ_1 are the dip, strike and rake calculated using the inversion from the P and S amplitudes, δ_2, ϕ_2 and λ_2 are the dip, strike and rake calculated using the inversion from the P amplitudes only, α is the sum of deviations between slips and between fault normals of the two focal mechanisms, M is the magnitude of the event. The events with $\alpha > 25°$ have been discarded from the stress analysis, since their mechanisms were unreliable.

Table 2. Source parameters of the B type earthquakes.

No	Date (yymmdd)	Time (hh:mm:ss)	M	δ_1 (deg)	ϕ_1 (deg)	λ_1 (deg)	δ_2 (deg)	ϕ_2 (deg)	λ_2 (deg)	α (deg)	DC (per cent)	ISO (per cent)	CLVD (per cent)
21	970116	16:50:38	0.7	56	50	45	51	51	45	9	48.8	17.8	33.4
22	970117	05:30:58	0.8	74	38	45	71	39	38	10	61.3	15.0	23.7
23	970117	07:22:37	1.2	75	34	45	73	32	41	7	70.4	16.1	13.6
24	970117	09:09:52	0.9	54	60	48	49	64	50	8	52.0	19.0	29.0
25	970117	22:57:38	3.0	67	43	39	63	41	32	12	75.3	9.5	15.1
26	970117	23:04:35	1.2	68	50	42	26	84	93	84	57.3	20.3	22.4
27	970118	00:53:20	0.9	47	41	46	71	39	47	40	87.4	12.2	−0.5
28	970118	00:56:15	0.9	63	35	45	72	36	44	16	46.0	17.9	36.1
29	970118	01:08:11	1.2	57	46	51	67	43	50	17	43.9	17.3	38.8
30	970118	02:16:39	0.7	66	32	47	83	35	55	33	82.6	10.1	7.3
31	970118	05:34:15	2.3	65	41	34	68	41	32	5	45.8	3.3	50.9
32	970118	05:51:04	1.6	65	35	46	69	34	46	6	65.3	15.1	19.5
33	970118	05:55:32	1.0	60	45	49	65	44	47	8	51.8	15.4	32.9
34	970118	06:28:08	1.2	61	48	50	68	46	48	12	52.9	15.8	31.3
35	970118	09:58:08	1.9	70	40	49	60	36	41	22	65.0	13.0	22.0
36	970118	10:00:11	0.7	66	37	48	80	37	50	25	55.0	17.0	27.9
37	970118	19:21:01	0.7	63	35	46	60	34	45	6	49.5	17.8	32.7
38	970119	05:25:12	1.0	72	49	45	69	47	38	9	62.0	19.2	18.8
39	970119	14:57:14	0.8	54	35	48	58	31	47	6	41.1	19.7	39.1
40	970126	12:31:27	1.1	57	54	48	53	52	45	9	79.9	15.0	5.1
41	970126	14:45:58	1.6	70	33	42	64	29	31	18	72.7	12.2	15.1
42	970126	14:54:37	0.9	58	43	44	58	45	41	6	44.6	18.7	36.7
43	970127	00:32:04	2.0	65	37	49	72	37	51	13	62.8	14.0	23.2
44	970127	00:59:53	0.9	71	23	37	74	11	35	19	68.8	13.8	17.4
45	970127	13:25:14	0.8	64	33	47	74	35	51	20	62.3	15.8	21.8
46	970115	12:51:21	1.2	82	35	46	86	36	50	9	93.4	5.4	1.2
47	970115	21:02:58	0.7	86	20	39	89	29	49	23	97.2	2.0	0.7
48	970116	09:54:14	0.9	90	18	40	89	207	−49	21	84.5	9.2	6.4
49	970118	06:38:29	1.2	80	21	43	87	16	42	9	62.2	17.8	20.0

For meaning of the quantities, see Table 1. The B earthquakes with nos 46–49 were originally denoted as earthquakes of type AB by Horálek *et al.* (2000b, Table 3).

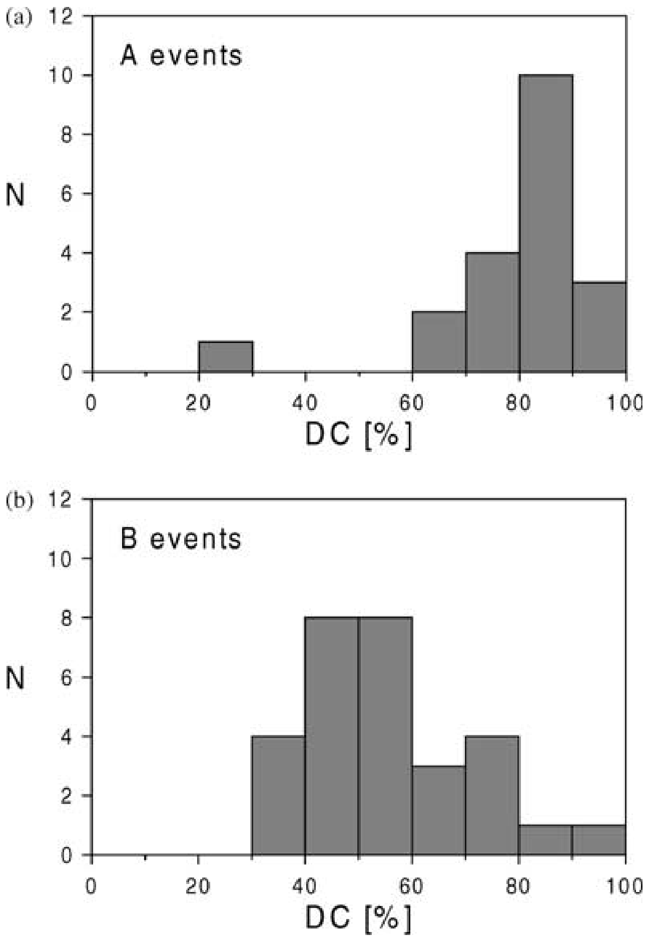

Figure 3. Percentages of the DC component in the type A (a) and type B (b) events.

combination of DC tensors can produce the non-zero ISO (Julian *et al.* 1998).

The indication concerning the ISO components helps to resolve whether the B events are complex shear events or not. Comparison of the ISO components of the A and B events (see Tables 1 and 2) shows that the ISO component in the B events is significantly higher then that in the A events. This clearly contradicts the proposed interpretation. Furthermore, complexities of the *P* and *S* waveforms of the A and B events are comparable, hence there is no indication that the source process of the B events is more complex than that of the A events.

4.2 Shear faulting in a heterogeneous or anisotropic medium

Shear earthquakes may also appear to have non-DC components if the focal area is heterogeneous. If earthquakes occur in a place where the elastic moduli vary spatially, the spatial derivatives of the Green function may vary significantly over the source region. In this case, the distortion of the focal mechanism is caused by the finiteness of the source region rather than by a non-planar geometry of the fault (Julian *et al.* 1998).

Another cause of non-DC components may be anisotropy of the medium in the focal area. Shear faulting in an anisotropic medium has a different equivalent force system than it would if the medium were isotropic. A shear faulting in an anisotropic medium generally produces a non-DC moment tensor (Julian *et al.* 1998). This also applies in the case when correct Green functions for the anisotropic medium are used to solve the inverse problem. Shear faulting in a medium with orthorhombic symmetry was studied, for example, by Kawasaki & Tanimoto (1981).

One can suspect that anisotropy produces the non-DC components in earthquakes in West Bohemia, because Vavryčuk (1993) reported on a 6 per cent anisotropy in the region. Nevertheless, it seems that neither anisotropy nor heterogeneity at the source caused the appearance of non-DC components in the earthquakes. The foci of the A and B events occupied a very small area characterized very probably by the same elastic properties. Also raypaths to stations were almost identical for both types of events. Therefore, the effects of anisotropy or heterogeneity should appear in the B as well as A events but not in the B events only.

4.3 Tensile faulting owing to high pore fluid pressure

Tensile faulting is characterized by the displacement discontinuity, which is not parallel to a fault surface. This type of faulting is typical for geothermal and volcanic regions (Julian *et al.* 1997; Ross *et al.* 1996) and causes non-DC mechanisms. Tensile faulting is permissible only under a high pore fluid pressure, because fluid pressure can cancel out the compressive lithostatic stress acting against opening of cracks at depth in the Earth (Julian *et al.* 1998). Pore fluid pressure is assumed to significantly influence the seismicity pattern and the type of faulting (Henderson & Maillot 1997; Yamashita 1997). The pore fluid pressure decreases the effective stress on faults, destabilizes faults and triggers earthquakes. If the ratio of pore pressure to lithostatic stress exceeds 0.6 then it can cause tensile faulting, which is also called hydrofracturing (Byerlee 1990). Fluid pressures comparable to the lithostatic stress are found surprisingly often in deep boreholes (Julian *et al.* 1998). A fluid pressure higher than the hydrostatic pressure is called overpressure and is explained by a low permeability of the rock in which the fluid is trapped (Byerlee 1990; Hardebeck & Hauksson 1999).

Since West Bohemia is a geothermal area, in which a high fluid pressure is a reasonably satisfied assumption, the tensile faulting owing to high fluid pressure may explain the non-DC earthquakes under study. The high fluid pressure is also probably a key factor in generating the seismic activity with a typical swarm character in the area (Špičák *et al.* 1999; Špičák 2000). Tensile faulting is also indicated by positive values of the ISO and CLVD components observed in the non-DC (type B) events. However, it is not clear why DC (type A) earthquakes also occurred in the same area. Understanding this requires the determination of the tectonic stress, estimating the fluid pressure and calculating tractions generated along the faults by the effective stress. The differences in faulting of the A and B events should then be explained by differences in shear and normal tractions along the faults.

5 TECTONIC STRESS

5.1 Method

Tectonic stress is determined from focal mechanisms by applying the Gephart–Forsyth inversion method (Gephart & Forsyth 1984; Michael 1987; Gephart 1990; Plenefisch & Bonjer 1997; Lund & Slunga 1999). This method assumes that: (1) the stress is uniform in the region; (2) the earthquakes occur on pre-existing faults with varying orientations; and (3) the slip vector points in the direction of the resolved shear traction on the fault. The stress tensor is searched by minimizing the sum of deviations between the shear traction directions and the observed slips at the faults. The misfit function is minimized by using the robust grid search inversion scheme. Since this approach is purely geometric, we cannot recover the full stress tensor (six parameters) but only its part (four parameters): three angles defining the directions of the three principal stress axes and the parameter R. This parameter is called the shape ratio and bounds the size of the maximum, intermediate and minimum principal stresses σ_1, σ_2 and σ_3: $R = (\sigma_1 - \sigma_2)/(\sigma_1 - \sigma_3)$. The method is unable to recover the magnitudes of the principal stresses and the isotropic part of the stress tensor $\sigma^{\mathrm{ISO}} = \sigma_1 + \sigma_2 + \sigma_3$. Therefore, the stress tensor is searched with fixed maximum compressive stress $\sigma_1 = +1$ and with a zero isotropic part $\sigma^{\mathrm{ISO}} = 0$. Hence, only the directions of the three principal stress axes and the magnitude of the intermediate stress σ_2 ($\sigma_3 = -\sigma_1 - \sigma_2$) are varied during the grid search.

5.2 Data

If the mechanisms used in the inversion are determined accurately and the orientation of the fault planes is known, the inversion method by Gephart & Forsyth (1984) produces reliable results. If the fault plane orientations are not available, the method can still produce some values of stress but with smaller resolution (Michael 1987). Therefore, the mechanisms of A and B events calculated by Horálek *et al.* (2000b) were used in the inversion, because their fault planes were determined from clustering of foci (see Fig. 2). Furthermore, from the whole set of A and B events (see Tables 1 and 2) only the most reliable mechanisms were applied in the inversion in order to improve the accuracy of the results. For this purpose, the quality of the mechanisms was estimated by comparing orientations of nodal planes calculated using two different moment tensor inversions: inversion performed from both *P* and *S* amplitudes (Dahm *et al.* 2000), and inversion performed from *P* amplitudes only. This comparison shows (see Tables 1 and 2) that the mechanisms calculated using the two methods are very similar for the majority of events. The average deviation of the fault orientation is 10.4°, the average deviation in the slip direction is 12.0°. This indicates that the results of the inversions are very stable and plausible for most of the events. However, several events display significantly different mechanisms for the two inversions. This is an indication that these mechanisms are problematic. In order to exclude the anomalous cases, only the events yielding sums of the deviations between the fault and slip orientations of less than or equal to 25° were retained. This condition was satisfied for 40 events: 14 type A events and 26 type B events; nine events were discarded (see Tables 1 and 2). In the new data set, the average deviation of the fault orientation is 6.3°, and the average deviation in the slip direction is 5.7°. Hence the accuracy of the focal mechanisms for the new data set is significantly increased. The selection criterion excluded, for example, A event no 15 with an anomalously biased DC component (32 per cent) and B event no 27, which was the only B event with a compressive CLVD.

5.3 Orientation of principal stresses

The inversion for the optimum stress tensor was performed using a 2° grid in searching through the principal stress directions and a 0.01 increment in searching for σ_2. The optimum principal stress directions are (plunge/azimuth): $\sigma_1 = 33°/156°$, $\sigma_2 = 48°/20°$, $\sigma_3 = 23°/262°$ and the shape ratio is $R = 0.69$ (see Fig. 4). The azimuth is measured from north and the plunge from the horizontal plane. The average deviation angle is 4.9°. The minimum of the misfit function is very shallow, hence the error of the stress directions is estimated to be ~10° in azimuth and ~5° in plunge (see Fig. 5, upper plot). The error of the shape ratio is up to 0.15 (see Fig. 5, lower plot).

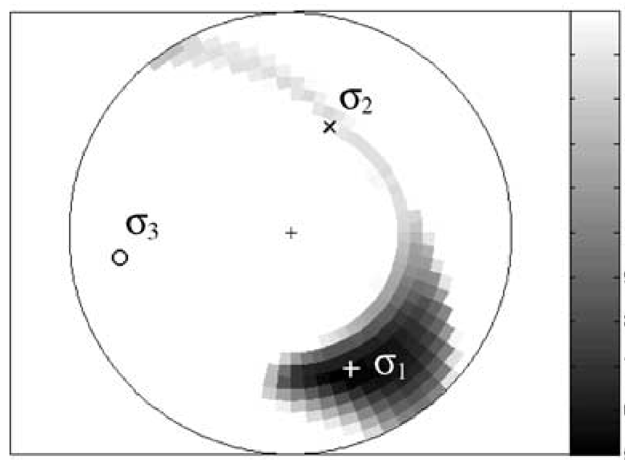

Figure 4. Inversion for stress. The misfit function for the σ_1 direction (average of deviations between the slip and shear traction on the fault measured in degrees) is displayed for the whole lower hemisphere. The equal-area projection is used.

5.4 Orientation of principal stresses obtained by other methods

The resolved stress is consistent with results obtained using other methods and other data in the same region or in the adjacent areas (see Table 3). The stress is very close to that obtained by Vavryčuk (2001, Fig. 17) who applied the same inversion method to a similar data set but using a 5° grid in searching for stress directions and a 0.05 increment in searching for σ_2. Similar results of those presented here were also obtained by Vavryčuk (2000), who applied the same method but using moment tensors from all 70 earthquakes analysed by Dahm *et al.* (2000) and Horálek *et al.* (2000b). However, the results of Vavryčuk (2000) are probably not very accurate because no information concerning the orientation of fault planes was utilized in the inversion. Consistent results were also obtained by Havíř (2000) who determined the stress in the same region and time period but used the program BRUTE3 (Hardcastle & Hills 1991) and a smaller set of mechanisms (see Havíř 2000, Table 3). The azimuth of the resolved maximum compressive stress also coincides well with the mean orientation of the stress in the KTB scientific drill hole (Brudy *et al.* 1997): N160°E ± 10° for the depth interval from 3.2 to 8.6 km. The resolved maximum compressive stress is also consistent with the mean stress orientation in Western Europe (Müller *et al.* 1992): N144°E ± 26°.

5.5 Estimation of absolute stress values

From the stress orientation and the shape ratio, we can infer the absolute values of the stress, which are important for estimation of pore fluid pressure or frictional parameters on faults. For a rough estimation of the absolute stress, values of the lithostatic stress $\sigma_z = 250$ MPa ($\sigma_z = \rho g z$, $\rho = 2800$ kg m^{-3}, $g = 9.81$ m s^{-2}, $z = 9000$ m)

Table 3. Orientation of principal stress axes in the focal and adjacent areas.

	Site	σ_1 (pl/az)	σ_2 (pl/az)	σ_3 (pl/az)	R
This paper	**West Bohemia**	**33°/156°**	**48°/20°**	**23°/262°**	**0.69**
Vavryčuk (2001)	West Bohemia	35°/160°	48°/19°	20°/265°	0.76
Vavryčuk (2000)	West Bohemia	30°/145°	55°/1°	17°/245°	0.58
Havíř (2000)	West Bohemia	∼33°/157°	—	∼30°/269°	∼0.9
Brudy *et al.* (1997)	KTB	0°/160° ± 10°	Vertical	0°/250° ± 10°	0.72
Müller *et al.* (1992)	Western Europe	0°/144° ± 26°	Vertical	0°/234° ± 26°	—

The bold values of stress are considered to be optimum for the 1997 January West Bohemia earthquake swarm.

and of the maximum compressive stress $\sigma_1 = 350$ MPa (see Plenefisch & Bonjer 1997, Fig. 10) were adopted. Taking into account these values and the resolved orientations of the principal stresses and the shape ratio, we arrive at the following values for the intermediate and minimum stresses: $\sigma_2 = 220$ MPa and $\sigma_3 = 162$ MPa. The lithostatic (isotropic) pressure

$$\sigma^{\mathrm{ISO}} = \frac{1}{3}(\sigma_1 + \sigma_2 + \sigma_3) \tag{4}$$

attains a value of $\sigma^{\mathrm{ISO}} = 244$ MPa. Hence the lithostatic pressure is slightly less than the lithostatic stress (250 MPa). Note that the calculated stress values are only rough estimations, because the value of the maximum compressive stress was only guessed. Fig. 6 shows stresses σ_2, σ_3 and σ^{ISO} calculated under the assumption that σ_1 is not fixed but lies in the interval between 300 and 400 MPa. Interestingly, stresses σ_2 and σ_3 are quite sensitive to σ_1, but the lithostatic pressure σ^{ISO} is almost insensitive to σ_1. It implies that the pressure is determined with a good accuracy even though the absolute stresses σ_1, σ_2 and σ_3 are not well constrained.

The above stress values can be compared with the stress at the KTB drill hole, which is located 50 km SW of the epicentral area. The stress was measured at the KTB at the depth interval from 3 km to 6.8 km (see Brudy *et al.* 1997, Fig. 11). If we interpolate the measured stress to a depth of 9 km, at which the seismic activity occurred, we arrive at the following approximate values: $\sigma_1 = 380$ MPa, $\sigma_2 = 250$ MPa and $\sigma_3 = 200$ MPa. The shape ratio, $R = 0.72$, corresponds well to the resolved shape ratio in the focal area ($R = 0.69$). The pressure $\sigma^{\mathrm{ISO}} = 277$ MPa is higher than the lithostatic stress (250 MPa). All stresses σ_1, σ_2 and σ_3 are slightly higher than those obtained for the focal area.

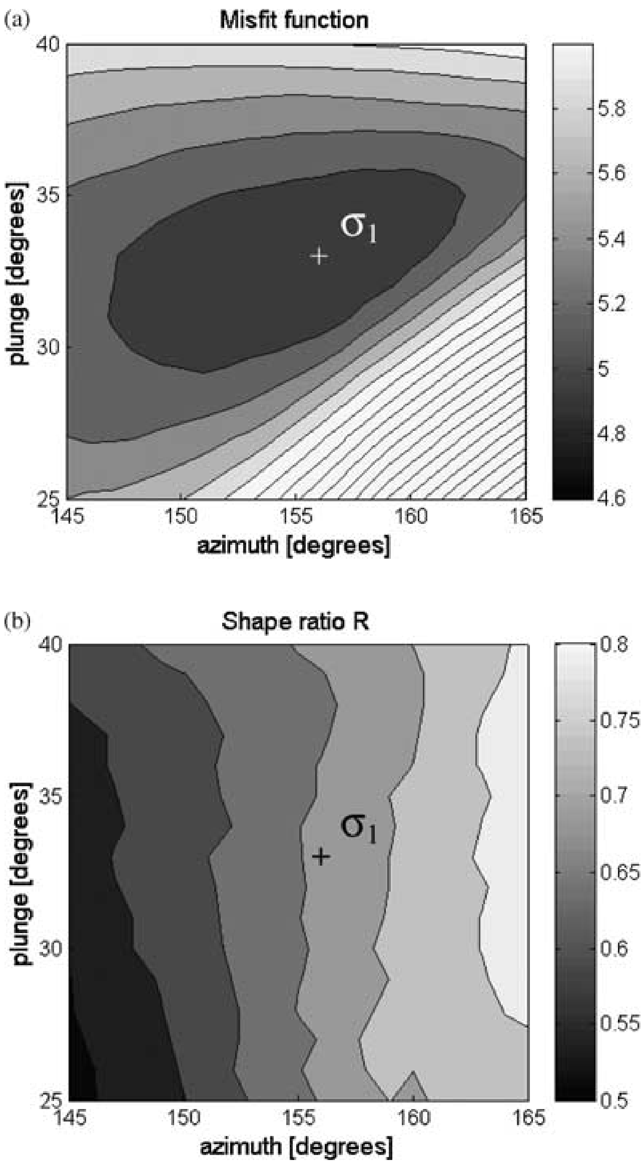

Figure 5. Maps of the misfit function (a) and of shape ratio R (b) for the σ_1 direction. The position of the optimum σ_1 direction is marked by the cross.

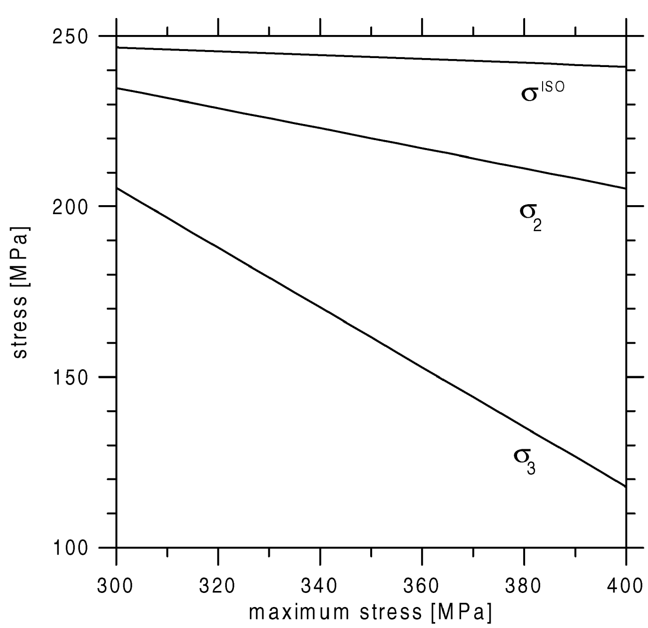

Figure 6. Minimum, intermediate and isotropic stresses as a function of maximum compressive stress σ_1.

6 SHEAR AND NORMAL TRACTIONS FOR DC AND NON-DC EARTHQUAKES

The A and B earthquakes were associated with two faults of different orientations and also displayed a different type of faulting. The A events were DC and the B events were non-DC. Understanding the differences in faulting requires calculating shear and normal tractions generated by the effective stress along the faults and correlating them with the non-DC components of the events.

6.1 Shear traction versus the DC component

The shear traction along the fault is calculated from the fault orientation and from the tectonic stress. Fig. 7 shows the shear traction versus the percentage of the DC for the 40 selected earthquakes under study. The figure indicates a clear correlation between the percentage of the DC and the value of the shear traction. Highly DC earthquakes are characterized by high values of shear traction and highly non-DC earthquakes are characterized by low values of shear traction. This observation is unique and it has not yet been reported on. It proves that the size of the DC and non-DC components in the earthquakes is controlled by the orientation of the fault with respect to the stress. High values of shear traction are generated on *optimally oriented* faults and result in shear faulting (A events). Low values of shear traction are generated on *misoriented* faults and result in faulting with a significant non-shear component (B events). Highly misoriented faults contain a high non-shear component.

The above observation supports the idea of tensile faulting. High shear traction on optimally oriented faults tends to generate DC earthquakes with the slip lying in the fault. Low shear traction indicates anomalous stress conditions on misoriented faults, which generate non-DC (tensile) earthquakes with the slip deviating from the fault. High values of the non-DC component indicate high deviations of the slip from the fault.

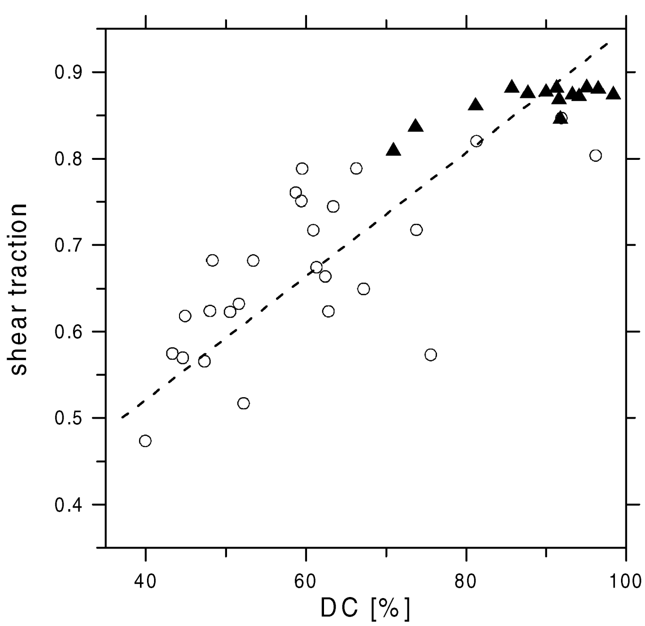

Figure 7. DC percentage for the A (triangles) and B (circles) type earthquakes versus normalized shear traction on the fault. The dashed line shows the linear interpolation of the data.

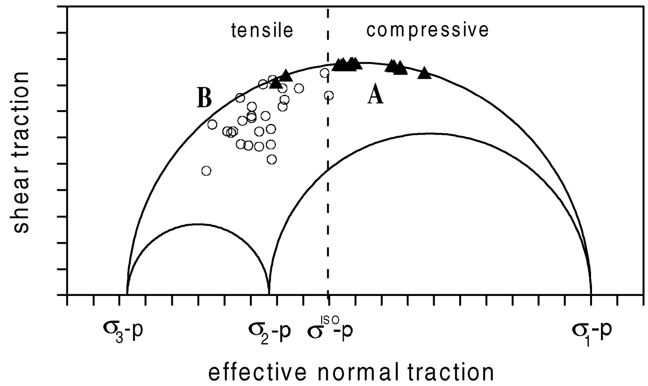

Figure 8. Mohr's circle stress diagram for the type A (triangles) and type B (circles) earthquakes. All permissible values of shear and normal traction must lie inside the large circle but outside of the smaller circles. The dashed line indicates the zero effective normal traction and separates areas with tensile and compressive stress regimes.

6.2 Determination of pore fluid pressure

The effective normal traction on the fault depends on the fault orientation, on the tectonic stress and on the pore fluid pressure. Unfortunately, the fluid pressure is not known in the focal area and it can only be speculated on. Nevertheless, we can set up limits for the fluid pressure requiring the normal traction to be consistent with the earthquake mechanisms observed.

Fig. 8 shows Mohr's circle diagram (Jaeger & Cook 1979; Mavko *et al.* 1998) for the 40 selected earthquakes under study. This diagram displays the shear traction versus the effective normal traction, which is defined as the difference between the normal traction and the fluid pressure. The shear and normal tractions are calculated from the tectonic stress and from the fault orientations. The fluid pressure is unknown, hence the origin of the axis of the effective normal traction is not defined. For increasing values of fluid pressure, the origin of the axis moves from the left to the right.

The comparison of tractions for the type A and B earthquakes (Fig. 8) shows that these earthquakes are generated under different stress conditions on the fault. The shear traction is high for the A events and considerably lower for the B events. The shear traction is even close to its maximum available in the stress field for the A events. The effective normal traction is also significantly higher for the A events than for the B events. This observation is in accordance with the mechanisms of the events and can be exploited in estimation of the fluid pressure. Since the A events are shear and the B events are tensile, the effective normal traction should attain positive values (compressive force) for the A events but negative values (tensile force) for the B events. This constrains the position of the zero effective normal traction (Fig. 8, dashed line) and subsequently the value of the fluid pressure. The fluid pressure corresponds roughly to the lithostatic pressure in the focal area $\sigma^{\mathrm{ISO}} = \frac{1}{3}(\sigma_1+\sigma_2+\sigma_3)$, hence $p = 244$ MPa. This value is very stable being almost independent of the actual value of the maximum compressive stress used (see Fig. 6). The fluid pressure is less then the lithostatic stress by $\sim$5 MPa. The ratio of the fluid pressure to the maximum compressive stress is 0.7.

7 DISCUSSION

It was shown that shear as well as tensile earthquakes could occur simultaneously in the same focal area but on faults with different orientations. Interestingly, detecting such a mixed family of earthquakes is advantageous because it allows one to infer the fluid pressure at the area. If we assume that the fluid pressure is independent of the orientation of faults, we can determine the fluid pressure as follows. The fluid pressure should attain a value such that the effective normal traction will be compressive on the faults with shear earthquakes but extensive on the faults with tensile earthquakes. In other words, the fluid pressure must be high enough to induce tensile faulting on some favourably oriented faults but also low enough not to induce tensile faulting on the other faults. If the absolute value of the tectonic stress is known, this approach yields the absolute value of the fluid pressure p. If only the shape ratio R is known, then the *fluid ratio* defined as

$$R_P = \frac{\sigma_1 - p}{\sigma_1 - \sigma_3} \tag{5}$$

can be determined. Obviously, the fluid ratio is $R_P > 1$ for zero fluid pressure, and $R_P = 1$ for fluid pressure equal to σ_3. Tensile faulting can occur only for $p > \sigma_3$, which is equivalent to $R_P < 1$. The fluid ratio for the area under study is 0.56. Note that the estimation of fluid pressure or the fluid ratio requires no information concerning friction.

8 CONCLUSIONS

(1) Tensile faulting consistently explains non-DC earthquakes that occurred during the 1997 January West Bohemian earthquake swarm. The tensile earthquakes displayed low DC together with high positive ISO and CLVD. The tensile earthquakes were permissible owing to high fluid pressure in the source area.

(2) The tectonic stress in the West Bohemia region calculated from 40 accurately determined mechanisms of earthquakes that occurred during the 1997 January earthquake swarm is characterized by the following optimum values (plunge/azimuth): $\sigma_1 = 33°/156°$, $\sigma_2 = 48°/20°$, $\sigma_3 = 23°/262°$ and $R = 0.69 \pm 0.15$. The error of the stress directions is estimated to be $\sim 5°$ in plunge and $\sim 10°$ in azimuth. The azimuth of the maximum compressive stress coincides well with the mean orientation of the stress in the KTB drill hole (Brudy *et al.* 1997): N160°E $\pm$ 10° and with the mean orientation of the stress in Western Europe (Müller *et al.* 1992): N144°E $\pm$ 26°. However, the resolved maximum stress deviates from the horizontal direction. The absolute stress is estimated to be: $\sigma_1 = 350$ MPa, $\sigma_2 = 220$ MPa and $\sigma_3 = 162$ MPa. The lithostatic stress is 250 MPa.

(3) The percentage of the DC component in earthquakes clearly correlates with the magnitude of the shear traction along a fault. The DC earthquakes occurred along faults with high shear traction. The non-DC earthquakes occurred along faults with significantly reduced shear traction. This demonstrates that the tectonic stress primarily controlled the type of faulting.

(4) The DC earthquakes occurred on faults with high normal traction and non-DC earthquakes on faults with low normal traction. This supports the idea of the tensile nature of the non-DC earthquakes.

(5) The pore fluid pressure was estimated from the condition that the effective normal traction must be compressive for shear earthquakes but tensile for non-shear earthquakes. The fluid pressure is close to the lithostatic pressure in the area being approximately 244 MPa. Hence the fluid pressure is less than the lithostatic stress by $\sim$5 MPa. The ratio of the fluid pressure p to the maximum stress σ_1 is 0.7.

(6) The fluid ratio $R_P = (\sigma_1 - p)/(\sigma_1 - \sigma_3)$ was introduced to describe a relative value of the fluid pressure with respect to the tectonic stress. No absolute stress values are needed for evaluating the fluid ratio. The occurrence of tensile faulting is conditioned by the fluid ratio of less than 1. The fluid ratio in the area under study is 0.56.

ACKNOWLEDGMENTS

The author thanks Vladislav Babuška, Axel Plešinger, Alice Slancová and Aleš Špičák for critically reading the manuscript and for their comments, Günter Bock, Thorsten Dahm and an anonymous reviewer for their reviews, Jan Šílený for performing additional computations in order to test the accuracy of the mechanisms under study, and Alena Boušková for help with Fig. 1. This work was supported by the Grant Agency AS CR, grant no A3012904.

REFERENCES

Brudy, M., Zoback, M.D., Fuchs, K., Rummel, F. & Baumgärtner, J., 1997. Estimation of the complete stress tensor to 8 km depth in the KTB scientific drill holes: implications for crustal strength, *J. geophys. Res.,* **102,** 18 453–18 475.

Byerlee, J., 1990. Friction, overpressure and fault normal compression, *Geophys. Res. Lett.,* **17,** 2109–2112.

Dahm, T., Horálek, J. & Šílený, J., 2000. Comparison of absolute and relative moment tensor solutions for the January 1997 West Bohemia earthquake swarm, *Stud. Geophys. Geod.,* **44,** 233–250.

Dudek, A., 1987. Geology and tectonic pattern of the Western Bohenia seismic area, in *Earthquake Swarm 1985/86 in Western Bohemia,* Geophys. Inst. Czechosl. Acad. Sci., Praha, pp. 34–37.

Feigneir, B. & Young, R.P., 1992. Moment tensor inversion of induced microseismic events: evidence of non-shear failures in the $-4 < M < -2$ moment magnitude range, *Geophys. Res. Lett.,* **19,** 1503–1506.

Fischer, T. & Horálek, J., 2000. Refined locations of the swarm earthquakes in the Nový Kostel focal zone and spatial distribution of the January 1997 swarm in Western Bohemia, Czech Republic, *Stud. Geophys. Geod.,* **44,** 210–226.

Frohlich, C., 1994. Earthquakes with non-double-couple mechanisms., *Science,* **264,** 804–809.

Gephart, J.W., 1990. Stress and the direction of slip on fault planes, *Tectonics,* **9,** 845–858.

Gephart, J.W. & Forsyth, D.W., 1984. An improved method for determining the regional stress tensor using earthquake focal mechanism data: application to the San Fernando earthquake sequence, *J. geophys. Res.,* **89,** 9305–9320.

Hardcastle, K.C. & Hills, L.S., 1991. BRUTE3 and SELECT: Quickbasic 4 programs for the determination of stress tensor configuration and separation of homogeneous populations of fault-slip data, *Comput. Geosci.,* **17,** 23–43.

Hardebeck, J.L. & Hauksson, E., 1999. Role of fluids in faulting inferred from stress field signatures, *Science,* **285,** 236–239.

Hasegawa, H.S. & Kanamori, H., 1987. Source mechanism of the magnitude 7.2 Grand Banks earthquake of November 1929: double couple or submarine landslide?, *Bull. seism. Soc. Am.,* **77,** 1984–2004.

Havíř, J., 2000. Stress analyses in the epicentral area of Nový Kostel (Western Bohemia), *Stud. Geophys. Geod.,* **44,** 522–536.

Henderson, J.R. & Maillot, B., 1997. The influence of fluid flow in fault zones on patterns of seismicity: a numerical investigation, *J. geophys. Res.,* **102,** 2915–2924.

Horálek, J., Fischer, T., Boušková, A. & Jedlička, P., 2000a. The Western Bohemia/Vogtland region in the light of the WEBNET network., *Stud. Geophys. Geod.,* **44,** 107–125.

Horálek, J., Šílený, J., Fischer, T., Slancová, A. & Boušková, A., 2000b. Scenario of the January 1997 West Bohemia earthquake swarm, *Stud. Geophys. Geod.,* **44,** 491–521.

Jaeger, J.C. & Cook, N.G.W., 1979. *Fundamentals of Rock Mechanics,* Chapman and Hall, New York.

Jost, M.L. & Hermann, R.B., 1989. A student's guide to and review of moment tensors, *Seismol. Res. Lett.,* **60,** 37–57.

Julian, B.R., Miller, A.D. & Foulger, G.R., 1997. Non-double-couple earthquake mechanisms at the Hengill–Grensdalur volcanic complex, southwest Iceland, *Geophys. Res. Lett.,* **24,** 743–746.

Julian, B.R., Miller, A.D. & Foulger, G.R., 1998. Non-double-couple earthquakes 1: Theory, *Rev. Geophys.,* **36,** 525–549.

Kawasaki, I. & Tanimoto, T., 1981. Radiation patterns of body waves due to the seismic dislocation occurring in an anisotropic source medium, *Bull. seism. Soc. Am.,* **71,** 37–50.

Knopoff, L. & Randall, M.J., 1970. The compensated linear vector dipole: a possible mechanism for deep earthquakes, *J. geophys. Res.,* **75,** 4957–4963.

Kuge, K. & Lay, T., 1994. Data-dependent non-double-couple components of shallow earthquake source mechanisms: effects of waveform inversion instability, *Geophys. Res. Lett.,* **21,** 9–12.

Lund, B. & Slunga, R., 1999. Stress tensor inversion using detailed microearthquake information and stability constraints: application to Ölfus in southwest Iceland, *J. geophys. Res.,* **104,** 14 947–14 964.

Mavko, G., Mukerji, T. & Dvorkin, J., 1998. *The Rock Physics Handbook,* Cambridge University Press, Cambridge.

Michael, A.J., 1987. Use of focal mechanisms to determine stress: a control study, *J. geophys. Res.,* **92,** 357–368.

Miller, A.D., Foulger, G.R. & Julian, B.R., 1998. Non-double-couple earthquakes 2: Observations, *Rev. Geophys.,* **36,** 551–568.

Mori, J. & McKee, C., 1987. Outward-dipping ring-fault structure at Rabaul caldera as shown by earthquake locations, *Science,* **235,** 193–195.

Müller, B., Zoback, M.L., Fuchs, K., Mastin, L., Gregersen, S., Pavoni, N., Stephansson, O. & Ljunggren, C., 1992. Regional patterns of tectonic stress in Europe, *J. geophys. Res.,* **97,** 11 783–11 803.

Plenefisch, T. & Bonjer, K.P., 1997. The stress field in the Rhine Graben area inferred from earthquake focal mechanisms and estimation of frictional parameters, *Tectonophysics,* **275,** 71–97.

Ross, A.G., Foulger, G.R. & Julian, B.R., 1996. Non-double-couple earthquake mechanisms at the Geysers geothermal area, California, *Geophys. Res. Lett.,* **23,** 877–880.

Rudajev, V. & Šílený, J., 1985. Seismic events with non-shear components, II, Rockbursts with implosive source component, *Pure appl. Geophys.,* **123,** 17–25.

Šílený, J., 1997. Moment tensor rate functions from waveforms with non-homogeneous variance, *Geophys. J. Int.,* **131,** 767–769.

Šílený, J., 1998. Earthquake source parameters and their confidence regions by a genetic algorithm with 'memory', *Geophys. J. Int.,* **134,** 228–242.

Šílený, J. & Vavryčuk, V., 2000. Approximate retrieval of the point source in anisotropic media: numerical modelling by indirect parametrization of the source, *Geophys. J. Int.,* **143,** 700–708.

Sipkin, S.A., 1986. Interpretation of non-double-couple earthquake mechanisms derived from moment tensor inversion, *J. geophys. Res.,* **91,** 531–547.

Špičák, A., 2000. Earthquake swarm and accompanying phenomena in intraplate regions: a review, *Stud. Geophys. Geod.,* **44,** 89–106.

Špičák, A., Horálek, J., Boušková, A., Tomek, Č. & Vaněk, J., 1999. Magma intrusions and earthquake swarm occurrence in the western part of the Bohemian Massif, *Stud. Geophys. Geod.,* **43,** 87–106.

Vavryčuk, V., 1993. Crustal anisotropy from local observations of shear-wave splitting in West Bohemia, Czech Republic, *Bull. seism. Soc. Am.,* **83,** 1420–1441.

Vavryčuk, V., 2000. Comment on the 'Analysis of the state of stress during the 1997 earthquake swarm in Western Bohemia', eds Slancová, A. & Horálek, J., *Stud. Geophys. Geod.,* **44,** 614–619.

Vavryčuk, V., 2001. Inversion for parameters of tensile earthquakes, *J. geophys. Res.,* **106,** 16 339–16 355.

Weinlich, F.H., Tesař, J., Weise, S.M., Bräuer, K. & Kämpf, H., 1998. Gas flux distribution in mineral springs and tectonic structure in the western Eger Rift, *J. Czech Geol. Soc.,* **43,** 91–110.

Yamashita, T., 1997. Mechanical effect of fluid migration on the complexity of seismicity, *J. geophys. Res.,* **102,** 17 797–17 806.